Performance Analysis of a Microstrip Printed Antenna Conformed on a Cylindrical Body for TM_{10} mode Using Two Different Substrates

Ali Elrashidi[1], Khaled Elleithy[2], Hassan Bajwa [3]

[1]Department of Computer and Electrical Engineering, University of Bridgeport, Bridgeport, CT 06604, USA (aelrashi@bridgeport.edu)
2Department of Computer and Electrical Engineering, University of Bridgeport, Bridgeport, CT 06604, USA (elleithy@bridgeport.edu)
3Department of Computer and Electrical Engineering, University of Bridgeport, Bridgeport, CT 06604, USA (hbjwa@bridgeport.edu)

Abstract Curvature has a great effect on fringing field of a microstrip antenna and consequently fringing field affects effective dielectric constant and then all antenna parameters. A new mathematical model for input impedance, return loss, voltage standing wave ratio and electric and magnetic fields is introduced in this paper. These parameters are given for TM_{10} mode and using two different substrate materials RT/duroid-5880 PTFE and K-6098 Teflon/Glass. Experimental results for RT/duroid-5880 PTFE substrate are also introduced to validate the new model.

Keywords Fringing field, Curvature, effective dielectric constant and Return loss (S11), Voltage Standing Wave Ratio (VSWR), Transverse Magnetic TM_{10} mode.

1. Introduction

Due to the unprinted growth in wireless applications and increasing demand of low cost solutions for RF and microwave communication systems, the microstrip flat antenna, has undergone tremendous growth recently. Though the models used in analyzing microstrip structures have been widely accepted, the effect of curvature on dielectric constant and antenna performance has not been studied in detail. Low profile, low weight, low cost and its ability of conforming to curve surfaces [1], conformal microstrip structures have also witnessed enormous growth in the last few years. Applications of microstrip structures include Unmanned Aerial Vehicle (UAV), planes, rocket, radars and communication industry [2]. Some advantages of conformal antennas over the planer microstrip structure include, easy installation (randome not needed), capability of embedded structure within composite aerodynamic surfaces, better angular coverage and controlled gain, depending upon shape [3, 4]. While Conformal Antenna provide potential solution for many applications, it has some drawbacks due to bedding [5]. Such drawbacks include phase, impedance, and resonance frequency errors due to the stretching and compression of the dielectric material along the inner and outer surfaces of conformal surface. Changes in the dielectric constant and material thickness also affect the performance of the antenna. Analysis tools for conformal arrays are not mature and fully developed [6]. Dielectric materials suffer from cracking due to bending and that will affect the performance of the conformal microstrip antenna.

2. Background

Conventional microstrip antenna has a metallic patch printed on a thin, grounded dielectric substrate. Although the patch can be of any shape, rectangular patches, as shown in Figure 1 [7], are preferred due to easy calculation and modeling.

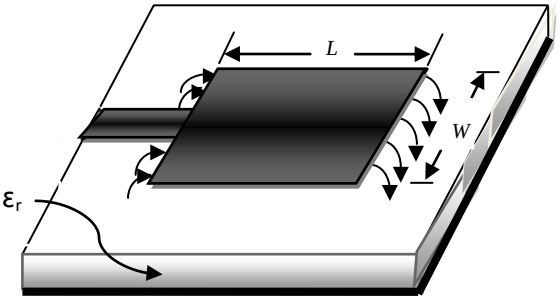

Figure 1. Rectangular microstrip antenna

Fringing fields have a great effect on the performance of a microstrip antenna. In microstrip antennas the electric filed in the center of the patch is zero. The radiation is due to the fringing field between the periphery of the patch and the ground plane. For the rectangular patch shown in the Figure 2, there is no field variation along the width and thickness. The amount of the fringing field is a function of the dimensions of the patch and the height of the substrate. Higher the substrate, the greater is the fringing field.

Due to the effect of fringing, a microstrip patch antenna would look electrically wider compared to its physical dimensions. As shown in Figure 2, waves travel both in

substrate and in the air. Thus an effective dielectric constant ε_{reff} is to be introduced. The effective dielectric constant ε_{reff} takes in account both the fringing and the wave propagation in the line.

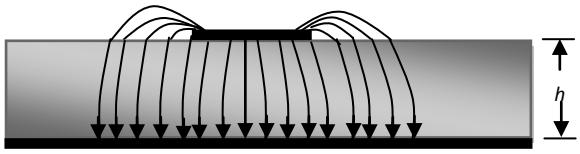

Figure 2. Electric field lines (Side View).

The expression for the effective dielectric constant is introduced by A. Balanis [7], as shown in Equation 1.

$$\varepsilon_{reff} = \frac{\varepsilon_r + 1}{2} + \frac{\varepsilon_r - 1}{2}\left[1 + 12\frac{h}{w}\right]^{-\frac{1}{2}} \quad (1)$$

The length of the patch is extended on each end by ΔL is a function of effective dielectric constant ε_{reff} and the width to height ratio (W/h). ΔL can be calculated according to a practical approximate relation for the normalized extension of the length [8], as in Equation 2.

$$\frac{\Delta L}{h} = 0.412\frac{(\varepsilon_{reff} + 0.3)\left(\frac{W}{h} + 0.264\right)}{(\varepsilon_{reff} - 0.258)\left(\frac{W}{h} + 0.8\right)} \quad (2)$$

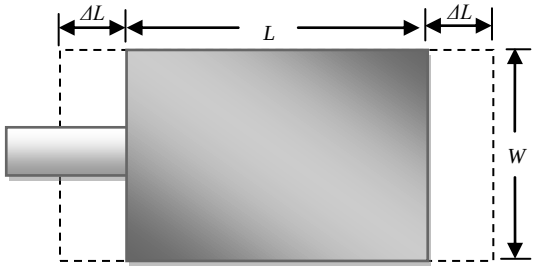

Figure 3. Physical and effective lengths of rectangular microstrip patch.

The effective length of the patch is L_{eff} and can be calculated as in Equation 3.

$$L_{eff} = L + 2\Delta L \quad (3)$$

By using the effective dielectric constant (Equation 1) and effective length (Equation 3), we can calculate the resonance frequency of the antenna f and all the microstrip antenna parameters.

Cylindrical-Rectangular Patch Antenna

All the previous work for a conformal rectangular microstrip antenna assumed that the curvature does not affect the effective dielectric constant and the extension on the length. The effect of curvature on the resonant frequency has been presented previously [9]. In this paper we present the effect of fringing field on the performance of a conformal patch antenna. A mathematical model that includes the effect of curvature on fringing field and on antenna performance is presented. The cylindrical rectangular patch is the most famous and popular conformal antenna. The manufacturing of this antenna is easy with respect to spherical and conical antennas.

Effect of curvature of conformal antenna on resonant frequency been presented by Clifford M. Krowne [9, 10] as:

$$[(f]_r)_{mn} = \frac{1}{2\sqrt{\mu\varepsilon}}\sqrt{\left(\frac{m}{2\theta a}\right)^2 + \left(\frac{n}{2b}\right)^2} \quad (4)$$

Where $2b$ is a length of the patch antenna, a is a radius of the cylinder, 2θ is the angle bounded the width of the patch, ε represents electric permittivity and μ is the magnetic permeability as shown in Figure 4.

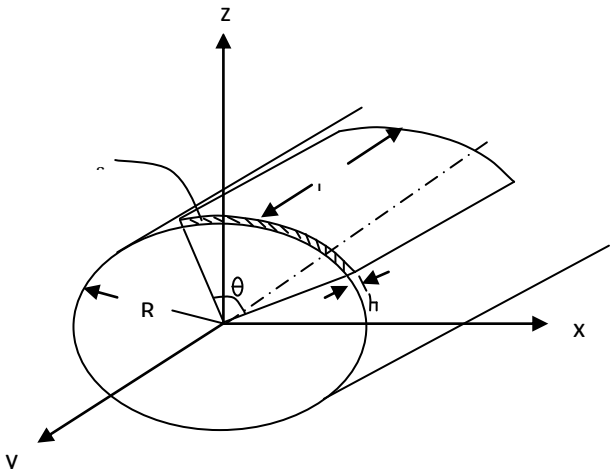

Figurer 4. Geometry of cylindrical-rectangular patch antenna[9]

Joseph A. *et al*, presented an approach to the analysis of microstrip antennas on cylindrical surface. In this approach, the field in terms of surface current is calculated, while considering dielectric layer around the cylindrical body. The assumption is only valid if radiation is smaller than stored energy[11]. Kwai *et al*. [12]gave a brief analysis of a thin cylindrical-rectangular microstrip patch antenna which includes resonant frequencies, radiation patterns, input impedances and Q factors. The effect of curvature on the characteristics of TM_{10} and TM_{01} modes is also presented in Kwai *et al*. paper. The authors first obtained the electric field under the curved patch using the cavity model and then calculated the far field by considering the equivalent magnetic current radiating in the presence of cylindrical surface. The cavity model, used for the analysis is only valid for a very thin dielectric. Also, for much small thickness than a wavelength and the radius of curvature, only *TM* modes are assumed to exist. In order to calculate the radiation patterns of cylindrical-rectangular patch antenna. The authors introduced the exact Green's function approach. Using Equation (4), they obtained expressions for the far zone electric field components E_θ and E_φ as a functions of Hankel function of the second kind $H_p^{(2)}$. The input impedance and Q factors are also calculated under the same conditions.

Based on cavity model, microstrip conformal antenna on a projectile for GPS (Global Positioning System) device is designed and implemented by using perturbation theory is

introduced by Sun L., Zhu J., Zhang H. and Peng X [13]. The designed antenna is emulated and analyzed by IE3D software. The emulated results showed that the antenna could provide excellent circular hemisphere beam, better wide-angle circular polarization and better impedance match peculiarity.

Nickolai Zhelev introduced a design of a small conformal microstrip GPS patch antenna [14]. A cavity model and transmission line model are used to find the initial dimensions of the antenna and then electromagnetic simulation of the antenna model using software called FEKO is applied. The antenna is experimentally tested and the author compared the result with the software results. It was founded that the resonance frequency of the conformal antenna is shifted toward higher frequencies compared to the flat one.

The effect of curvature on a fringing field and on the resonance frequency of the microstrip printed antenna is studied in [15]. Also, the effect of curvature on the performance of a microstrip antenna as a function of temperature for TM_{01} and TM_{10} is introduced in [16], [17].

3. General Expressions for Electric and Magnetic Fields Intensities

In this section, we will introduce the general expressions of electric and magnetic field intensities for a microstrip antenna printed on a cylindrical body represented in cylindrical coordinates.
Starting from Maxwell's Equations, we can get the relation between electric field intensity *E* and magnetic flux density *B* as known by Faraday's law [18], as shown in Equation (2):

$$\nabla \times E = -\frac{\partial B}{\partial t} \tag{2}$$

Magnetic field intensity *H* and electric flux density *D* are related by Ampérés law as in Equation (3):

$$\nabla \times H = J + \frac{\partial D}{\partial t} \tag{3}$$

where *J* is the electric current density.

The magnetic flux density *B* and electric flux density *D* as a function of time *t* can be written as in Equation (4):

$$B(t) = \mu\, H\, e^{-j\omega t} \quad \text{and} \quad D(t) = \varepsilon\, E\, e^{-j\omega t} \tag{4}$$

where μ is the magnetic permeability and ε is the electric permittivity.
By substituting Equation (4) in Equations (2) and (3), we can get:

$$\nabla \times E = -j\omega\mu \mathrm{H} \quad \text{and} \quad \nabla \times H = j\omega\varepsilon E + J \tag{5}$$

where ω is the angular frequency and has the form of: $\omega = 2\pi f$. In homogeneous medium, the divergence of Equation (2) is:

$$\nabla . H = 0 \quad \text{and} \quad H = \nabla \times A \tag{6}$$

From Equation (5), we can get Equation (7):

$$\nabla \times E + j\omega\mu \mathrm{H} = 0 \quad \text{or} \quad \nabla \times (E + j\omega\mu \mathrm{A}) = 0 \tag{7}$$

Using the fact that, any curl free vector is the gradient of the same scalar, hence:

$$(E + j\omega\mu \mathrm{A}) = -\nabla\varphi \tag{8}$$

where φ is the electric scalar potential.

By letting: $\nabla . A = -j\omega\mu\varphi$

where *A* is the magnetic vector potential.
So, the Helmholtz Equation takes the form of (9):

$$\nabla^2 \mathrm{A} + k^2 = -\mathrm{J} \tag{9}$$

k is the wave number and has the form of: $k = \omega\sqrt{\mu\varepsilon}$, and ∇^2 is Laplacian operator. The solutions of Helmholtz Equation are called wave potentials:

$$E = -j\omega\mu\varepsilon A + \frac{1}{j\omega\varepsilon}\nabla(\nabla . \mathrm{A}) \tag{10}$$

$$H = \nabla \times A$$

3.1 Near Field Equations

By using the Equations number (10) and magnetic vector potential in [19], we can get the near electric and magnetic fields as shown below:

$$E_z = \frac{1}{2\pi j\omega\varepsilon} \sum_{n=-\infty}^{\infty} e^{jn\emptyset} \int_{-\infty}^{\infty} (k^2 - k_z^2) f_n(k_z) H_n^{(2)}\left(\rho\sqrt{k - k_z^2}\right) e^{jk_z z}\, dk_z \tag{12}$$

E_φ and E_ρ are also getting using Equation (7);

$$E_\emptyset = -\frac{1}{2\pi j\omega\varepsilon} \sum_{n=-\infty}^{\infty} e^{jn\emptyset} \int_{-\infty}^{\infty} k_z f_n(k_z) H_n^{(2)}\left(\rho\sqrt{k - k_z^2}\right) e^{jk_z z}\, dk_z \tag{13}$$

$$E_\rho = \frac{1}{2\pi j\omega\varepsilon} \sum_{n=-\infty}^{\infty} e^{jn\emptyset} \int_{-\infty}^{\infty} \sqrt{k^2 - k_z^2} f_n(k_z) H_n^{(2)'}\left(\rho\sqrt{k - k_z^2}\right) e^{jk_z z}\, dk_z \tag{14}$$

To get the magnetic field in all directions, we can use the second part of Equation (10) as shown below, where H_z= 0 for *TM* mode:

$$H_\emptyset = \frac{\partial\psi}{\partial\emptyset} = \frac{j}{2\pi} \sum_{n=-\infty}^{\infty} n e^{jn\emptyset} \int_{-\infty}^{\infty} f_n(k_z) H_n^{(2)}\left(\rho\sqrt{k - k_z^2}\right) e^{jk_z z}\, dk_z$$

(15)

$$H_\rho = -\frac{\partial \psi}{\partial \rho} = -\frac{1}{2\pi}\sum_{n=-\infty}^{\infty} e^{jn\emptyset} \int_{-\infty}^{\infty} f_n(k_z)\sqrt{k^2-k_z^2}H_n^{(2)'}\left(\rho\sqrt{k-k_z^2}\right) e^{jk_z z}\, dk_z$$

(16)

3.2 Far Field Equations

In case of far field, we need to represent the electric and magnetic field in terms of *r*, where *r* is the distance from the center to the point that we need to calculate the field on it. By using the cylindrical coordinate Equations, one can notice that a far field ρ tends to infinity when *r*, in Cartesian coordinate, tends to infinity. Also, using simple vector analysis, one can note that, the value of k_z will equal to $-k \times cos\theta$ [19], and from the characteristics of Hankel function, we can rewrite the magnetic vector potential illustrated in Equation (12) to take the form of far field as illustrated in Equation (17).

$$A_z \xrightarrow{r\to\infty} \frac{e^{-jkr}}{\pi r}\sum_{n=-\infty}^{\infty} e^{jn\emptyset} j^{n+1} f_n(-kcos\theta) \quad (17)$$

Hence, the electric and magnetic field can easily be calculated as shown below:

$$E_z = \frac{e^{-jkr}}{j\omega\varepsilon\pi r} k^2 \sum_{n=-\infty}^{\infty} e^{jn\emptyset} j^{n+1} f_n(-kcos\theta) \quad (18)$$

$$E_\emptyset = \frac{e^{-jkr}}{j\omega\varepsilon\pi r} \sum_{n=-\infty}^{\infty} jn\, e^{jn\emptyset} j^{n+1} f_n(-kcos\theta) \quad (19)$$

$$E_r = \frac{e^{-jkr}(1+jkr)}{j\omega\varepsilon\pi r^2} \sum_{n=-\infty}^{\infty} e^{jn\emptyset} j^{n+1} f_n(-kcos\theta) \quad (20)$$

The magnetic field intensity also obtained as shown below, where $H_z = 0$:

$$H_r = \frac{e^{-jkr}(1+jkr)}{r^2} \sum_{n=-\infty}^{\infty} e^{jn\emptyset} j^{n+1} f_n(-kcos\theta) \quad (21)$$

$$H_\emptyset = \frac{-e^{-jkr}}{\pi r} \sum_{n=-\infty}^{\infty} n\, e^{jn\emptyset} j^{n+2} f_n(-kcos\theta) \quad (22)$$

4. Input Impedance

The input impedance is defined as "the impedance presented by an antenna at its terminals" or "the ratio of the voltage current at a pair of terminals" or "the ratio of the appropriate components of the electric to magnetic fields at a point". The input impedance is a function of the feeding position as we will see in the next few lines.

To get an expression of input impedance Z_{in} for the cylindrical microstrip antenna, we need to get the electric field at the surface of the patch. In this case, we can get the wave equation as a function of excitation current density *J* as follow:

$$\frac{1}{\rho^2}\frac{\partial^2 E_\rho}{\partial \emptyset^2} + \frac{\partial^2 E_\rho}{\partial z^2} + k^2 E_\rho = j\omega\mu J \quad (23)$$

By solving this Equation, the electric field at the surface can be expressed in terms of various modes of the cavity as [15]:

$$E_\rho(z,\emptyset) = \sum_n \sum_m A_{nm}\psi_{nm}(z,\emptyset) \quad (24)$$

where A_{nm} is the amplitude coefficients corresponding to the field modes. By applying boundary conditions, homogeneous wave Equation and normalized conditions for ψ_{nm}, we can get an expression for ψ_{nm}as shown below:

1. ψ_{nm} vanishes at the both edges for the length *L*:

$$\frac{\partial \psi}{\partial z}\Big|_{z=0} = \frac{\partial \psi}{\partial z}\Big|_{z=L} = 0 \quad (25)$$

2. ψ_{nm} vanishes at the both edges for the width *W*:

$$\frac{\partial \psi}{\partial \emptyset}\Big|_{\emptyset=-\theta_1} = \frac{\partial \psi}{\partial \emptyset}\Big|_{\emptyset=\theta_1} = 0 \quad (26)$$

3. ψ_{nm} should satisfy the homogeneous wave Equation :

$$\left(\frac{1}{\rho^2}\frac{\partial^2}{\partial \emptyset^2} + \frac{\partial^2}{\partial z^2} + k^2\right)\psi_{nm} = 0 \quad (27)$$

4. ψ_{nm} should satisfy the normalized condition:

$$\int_{z=0}^{z=L}\int_{\emptyset=-\theta_1}^{\emptyset=\theta_1} \psi_{nm}\psi_{nm}^* = 1 \quad (28)$$

Hence, the solution of ψ_{nm}will take the form shown below:

$$\psi_{nm}(z,\emptyset) = \sqrt{\frac{\varepsilon_m\varepsilon_n}{2a\theta_1 L}}\cos\left(\frac{m\pi}{2\theta_1}(\emptyset-\emptyset_1)\right)\cos\left(\frac{n\pi}{L}z\right) \quad (29)$$

with

$$\varepsilon_p = \begin{cases} 1 & for\ p = 0 \\ 2 & for\ p \neq 0 \end{cases}$$

The coefficient A_{mn} is determined by the excitation current. For this, substitute Equation (29) into Equation (23) and multiply both sides of (23) by ψ^*_{nm}, and integrate over area of the patch. Making use of orthonormal properties of ψ_{nm}, one obtains:

$$A_{nm} = \frac{j\omega\mu}{k^2 - k_{nm}^2} \iint_{dim}^{feed} \psi^*_{nm} J_\rho \, d\emptyset dz \tag{30}$$

Now, let the coaxial feed as a rectangular current source with equivalent cross-sectional area $S_z \times S_\emptyset$ centered at$(Z_0, \emptyset_0)$, so, the current density will satisfy the Equation below:

$$J_\rho = \begin{cases} \frac{I_0}{S_z \times S_\emptyset} & Z_0 - \frac{S_z}{2} \le x \le Z_0 + \frac{S_z}{2} \\ & \emptyset_0 - \frac{S_\emptyset}{2} \le x \le \emptyset_0 + \frac{S_\emptyset}{2} \\ 0 & elsewhere \end{cases} \tag{31}$$

Use of Equation (31) in (30) gives:

$$A_{nm} = \frac{j\omega\mu l}{k^2 - k_{nm}^2} \sqrt{\frac{\varepsilon_m \varepsilon_n}{2a\theta_1 L}} \cos\left(\frac{m\pi}{2\theta_1}\emptyset_0\right) \cos\left(\frac{n\pi}{L} z_0\right) sinc\left(\frac{n\pi}{2L} z_0\right) sinc\left(\frac{m\pi}{2a\theta_1}\emptyset_0\right) \tag{32}$$

So, to get the input impedance, one can substitute in the following Equation:

$$Z_{in} = \frac{V_{in}}{I_0} \tag{33}$$

where V_{in} is the *RF* voltage at the feed point and defined as:

$$V_{in} = -E_\rho(z_0, \emptyset_0) \times h \tag{34}$$

By using Equations (24), (29), (32), (34) and substitute in (33), we can obtain the input impedance for a rectangular microstrip antenna conformal in a cylindrical body as in the following Equation:

$$Z_{in} = j\omega\mu h \sum_n \sum_m \frac{1}{k^2 - k_{nm}^2} \frac{\varepsilon_m \varepsilon_n}{2a\theta_1 L} \cos^2\left(\frac{m\pi}{2\theta_1}\emptyset_0\right) \cos^2\left(\frac{n\pi}{L} z_0\right) \times sinc\left(\frac{n\pi}{2L} z_0\right) sinc\left(\frac{m\pi}{2a\theta_1}\emptyset_0\right) \tag{35}$$

5. Voltage Standing Wave Ratio and Return Loss

Voltage Standing Wave Ration *VSWR* is defined as the ration of the maximum to minimum voltage of the antenna. The reflection coefficient ρ define as a ration between incident wave amplitude V_i and reflected voltage wave amplitude V_r, and by using the definition of a voltage reflection coefficient at the input terminals of the antenna Γ, as shown below:

$$\Gamma = \frac{Z_{input} - Z_0}{Z_{input} + Z_0} \tag{36}$$

where, Z_0 is the characteristic impedance of the antenna. If the Equation is solved for the reflection coefficient, it is found that, where the reflection coefficient ρ is the absolute vale of the magnitude of Γ,

$$\rho = |\Gamma| = \frac{VSWR - 1}{VSWR + 1} \tag{37}$$

Consequently,

$$VSWR = \frac{|\Gamma| + 1}{|\Gamma| - 1} \tag{38}$$

The characteristic can be calculated as in [14],

$$Z_0 = \sqrt{\frac{L}{C}} \tag{39}$$

where : L is the inductance of the antenna, and C is the capacitance and can be calculated as follow:

$$C = \frac{2\pi\varepsilon}{\ln\left(\frac{a+h}{a}\right)} \frac{W}{2\pi\varepsilon} \tag{40}$$

$$L = \frac{\mu}{2\pi} \ln\left(\frac{a+h}{a}\right) \frac{W}{2\pi\varepsilon} \tag{41}$$

Hence, we can get the characteristic impedance as shown below:

$$Z_0 = \frac{1}{2\pi} \sqrt{\frac{\mu}{\varepsilon}} \ln\left(\frac{a+h}{a}\right) \tag{42}$$

The return loss s_{11} is related through the following Equation:

$$s_{11} = -20 \log\left[\frac{V_r}{V_i}\right] = -20 \log\left[\frac{VSWR - 1}{VSWR + 1}\right] \tag{43}$$

6. Results

For the range of GHz, the dominant mode is TM_{10} for $h << W$ which is the case. Also, for the antenna operates at the ranges 2.49 and 2.23 GHz for two different substrates we can use the following dimensions; the original length is 41.5 cm, the width is 50 cm and for different lossy substrate we can get the effect of curvature on the effective dielectric constant and the resonance frequency.

Two different substrate materials RT/duroid-5880 PTFE and K-6098 Teflon/Glass are used for verifying the new model. The dielectric constants for the used materials are 2.2 and 2.5 respectively with a tangent loss 0.0015 and 0.002 respectively.

6.1 RT/duroid-5880 PTFE Substrate

The mathematical and experimental results for input impedance, real and imaginary parts for a different radius of curvatures are shown in Figures 5 and 6. The peak value of the real part of input impedance is almost 600 Ω at frequency 2.49 GHz which gives a zero value for the imaginary part of input impedance as shown in Figure 6 at 20 mm radius of curvature. The value 2.49 GHz represents a resonance frequency for the antenna at 20 mm radius of curvature.

VSWR is given in Figure 7. It is noted that, the value of VSWR is almost 1.4 at frequency 2.49 GHz which is very efficient in manufacturing process. It should be between 1 and 2 for radius of curvature 20 mm. The minimum VSWR we can get, the better performance we can obtain as shown clearly from the definition of VSWR.

Return loss (S11) is illustrated in Figure 8. We obtain a very low return loss, -12 dB, at frequency 2.49 GHz for radius of curvature 20 mm.

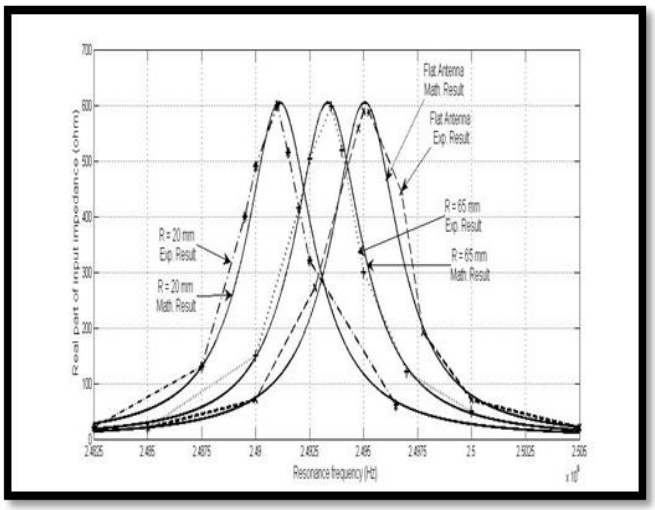

Figure 5. Mathimatical and experimental real part of the input impedance as a function of frequency for different radius of curvatures.

Normalized electric field for different radius of curvatures is illustrated in Figure 9. Normalized electric field is plotted for θ from zero to 2π and φ equal to zero. As the radius of curvature is decreasing, the radiated electric field is getting wider, so electric field at 20 mm radius of curvature is wider than 65 mm and 65 mm is wider than flat antenna. Electric field strength is increasing with decreasing the radius of curvature, because a magnitude value of the electric field is depending on the effective dielectric constant and the effective dielectric constant depending on the radius of curvature which decreases with increasing the radius of curvature.

Normalized magnetic field is wider than normalized electric field, and also, it is increasing with deceasing radius of curvature. Obtained results are at for θ from zero to 2π and φ equal to zero and for radius of curvature 20, 65 mm and for a flat microstrip printed antenna are shown in Figure 10. For different radius of curvature, the resonance frequency changes according to the change in curvature, so the given normalized electric and magnetic fields are calculated for different resonance frequency according to radius of curvatures.

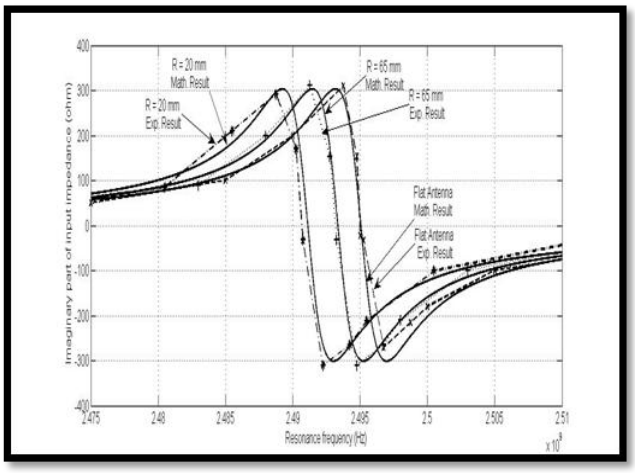

Figure 6. Mathimatical and experimental imaginary part of the input impedance as a function of frequency for different radius of curvatures.

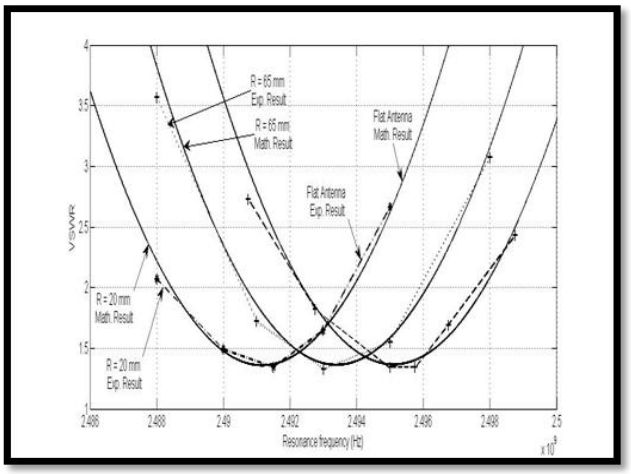

Figure 7. Mathimatical and experimental VSWR versus frequency for different radius of curvatures.

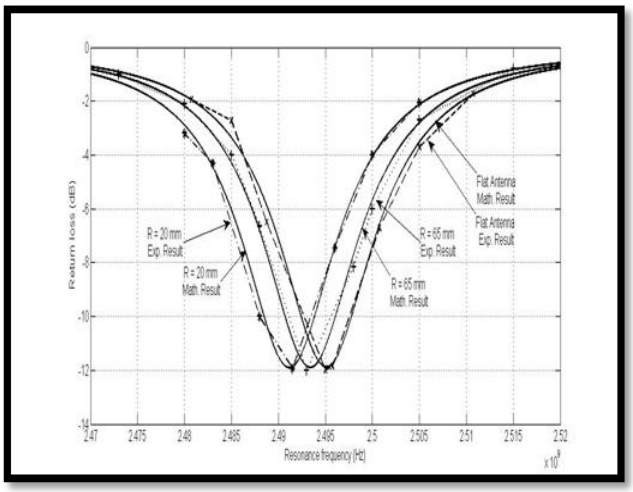

Figure 8. Mathimatical and experimental return loss (S11) as a function of frequency for different radius of curvatures.

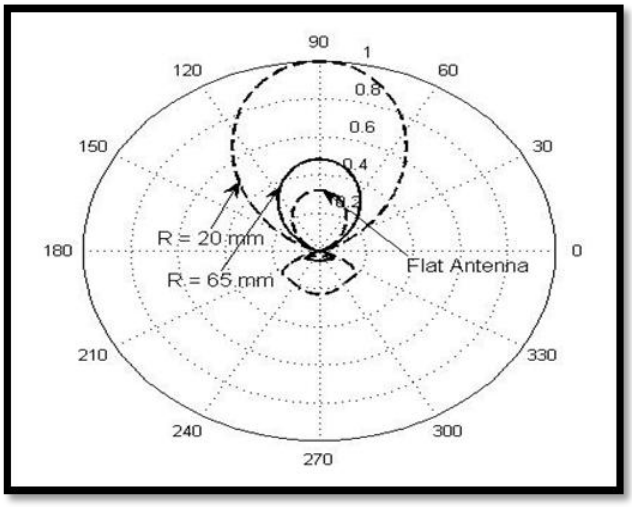

Figure 9. Normalized electric field for radius of curvatures 20, 65 mm and a flat antenna at θ=0:2π and φ=0^0.

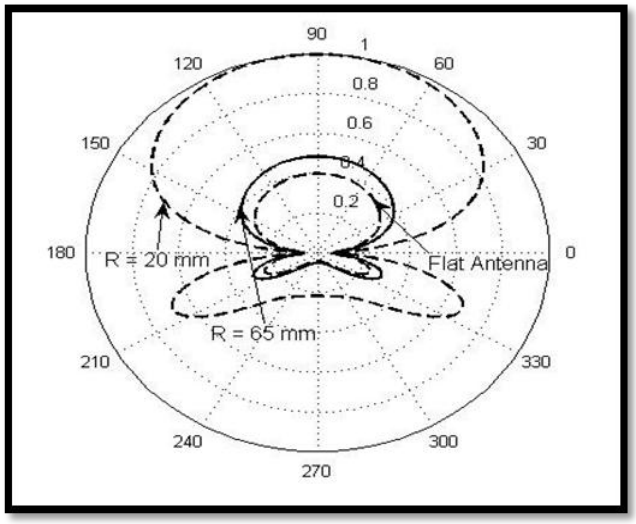

Figure 10. Normalized magnetic field for radius of curvatures 20, 65 mm and a flat antenna at θ=0:2π and φ=0^0.

6.2 K-6098 Teflon/Glass Substrate

The real part of input impedance is given in Figure 11 as a function of curvature for 20 and 65 mm radius of curvature compared to a flat microstrip printed antenna. The peak value of a real part of input impedance at 20 mm radius of curvature occurs at frequency 2.235 GHz at 410 Ω maximum value of resistance. The imaginary part of input impedance, Figure 12, is matching with the previous result which gives a zero value at this frequency. The resonance frequency at 20 mm radius of curvature is 2.235 GHz, which gives the lowest value of a VSWR, Figure 13, and lowest value of return loss as in Figure 14. Return loss at this frequency is -21 dB which is a very low value that leads a good performance for a microstrip printed antenna regardless of input impedance at this frequency.

The normalized electric field for K-6098 Teflon/Glass substrate is given in Figure 15 at different radius of curvatures 20, 65 mm and for a flat microstrip printed antenna.

Normalized electric field is calculated at θ equal to values from zero to 2π and φ equal to zero. At radius of curvature 20 mm, the radiation pattern of normalized electric field is wider than 65 mm and flat antenna, radiation pattern angle is almost 120^0, and gives a high value of electric field strength due to effective dielectric constant.

The normalized magnetic field is given in Figure 16, for the same conditions of normalized electric field. Normalized magnetic field is wider than normalized electric field for 20 mm radius of curvature; it is almost 170^0 for 20 mm radius of curvature. So, for normalized electric and magnetic fields, the angle of transmission is increased as a radius of curvature decreased.

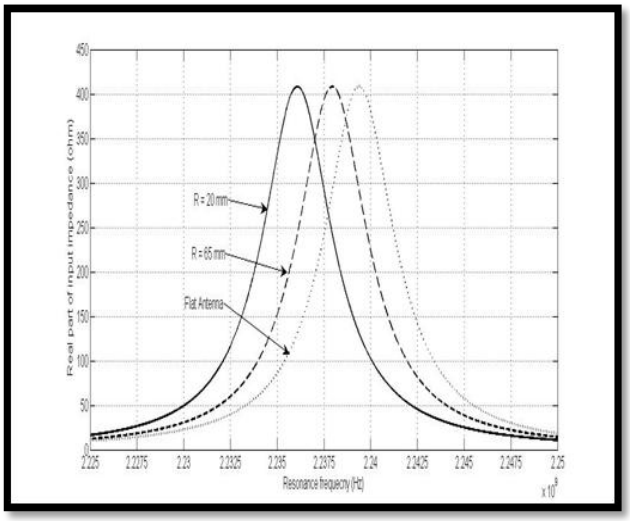

Figure 11. Real part of the input impedance as a function of frequency for different radius of curvatures.

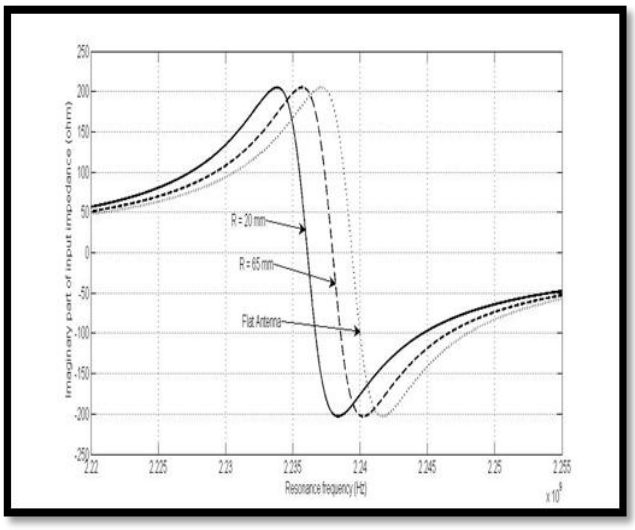

Figure 12. Imaginary part of the input impedance as a function of frequency for different radius of curvatures.

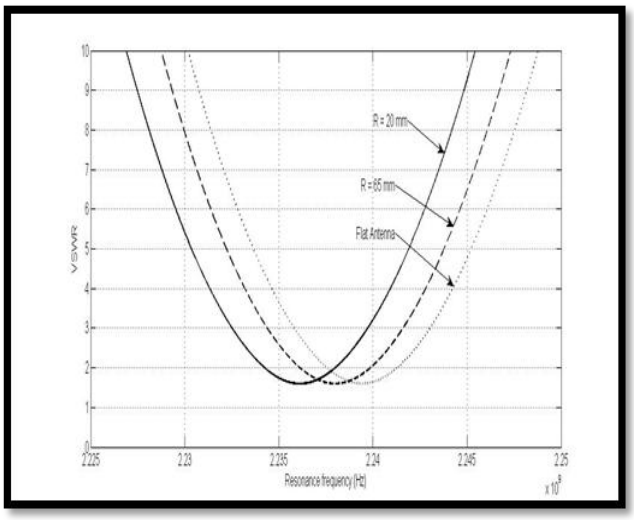

Figure 13. VSWR versus frequency for different radius of curvatures**.**

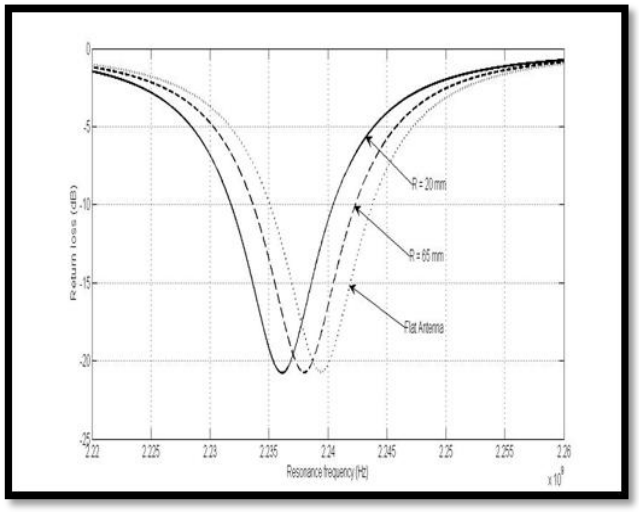

Figure 14. Return loss (S11) as a function of frequency for different radius of curvatures.

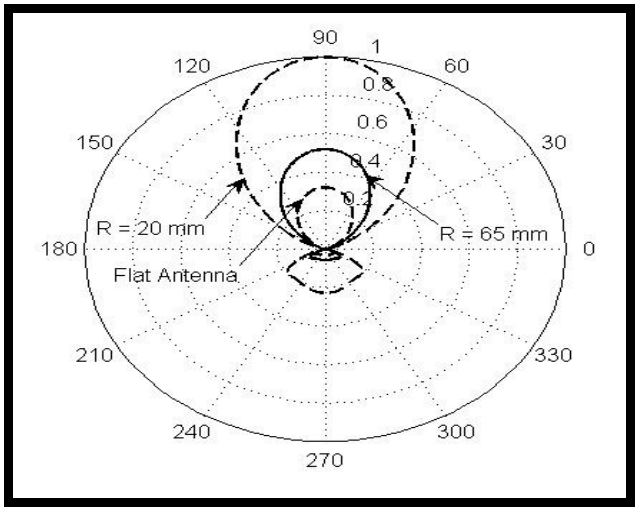

Figure 15. Normalized electric field for radius of curvatures 20, 65 mm and a flat antenna at $\theta=0:2\pi$ and $\varphi=0^0$.

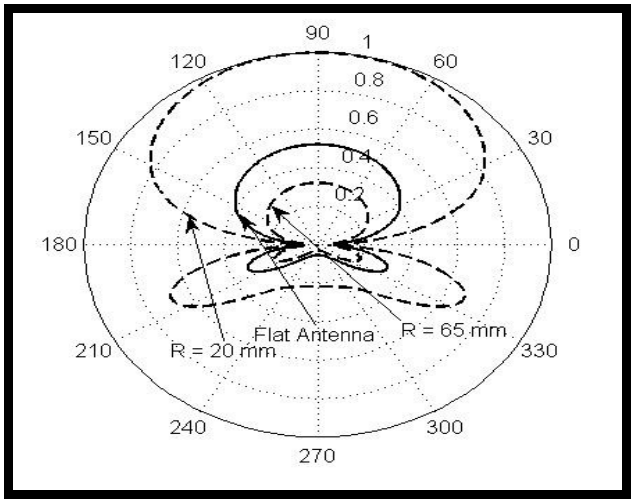

Figure 16. Normalized magnetic field for radius of curvatures 20, 65 mm and a flat antenna at $\theta=0:2\pi$ and $\varphi=0^0$.

7. Conclusion

The effect of curvature on the performance of conformal microstrip antenna on cylindrical bodies for TM_{10} mode is studied in this paper. Curvature affects the fringing field and fringing field affects the antenna parameters. The Equations for real and imaginary parts of input impedance, return loss, VSWR and electric and magnetic fields as a functions of curvature and effective dielectric constant are derived. By using these derived equations, we introduced the results for different dielectric conformal substrates. For the two dielectric substrates, the decreasing in frequency due to increasing in the curvature is the trend for all materials and increasing the radiation pattern for electric and magnetic fields due to increasing in curvature is easily noticed.

We conclude that, increasing the curvature leads to increasing the effective dielectric constant, hence, resonance frequency is increased. So, all parameters are shifted toward increasing the frequency with increasing curvature.

REFERENCES

[1] Heckler, M.V., et al., CAD Package to Design Rectangular Probe-Fed Microstrip Antennas Conformed on Cylindrical Structures. roceedings of the 2003 SBMO/IEEE MTT-S International, Microwave and Optoelectronics Conference, p p. 747-757, 2003.

[2] Q. Lu, X. Xu, and M. He, Application of Conformal FDTD Algorithm to Analysis of Conically Conformal Microstrip Antenna. IEEE International Conference on Microwave and Millimeter Wave Technology, ICMMT. , April 2008. p p. 527 – 530, 2008.

[3] Wong, K.L., Design of Nonplanar Microstrip Antennas and Transmission Lines. 1999: John & Sons, Inc, .

[4] Josefsson, L. and P. Persson, Conformal Array Antenna Theory and Design 1ed. 2006: Wiley-IEEE Press.

[5] Thomas, W., R.C. Hall, and D. I. Wu, Effects of curvature on the fabrication of wraparound antennas IEEE International Sym-

posium on Antennas and Propagation Society, pp. 1512-1515, 1997.

[6] J. Byun, B. Lee, and F.J. Harackiewicz, FDTD Analysis of Mutual Coupling between Microstrip Patch Antennas on Curved Surfaces. IEEE International Symposium on Antennas and Propagation Society, pp. 886-889, 1999.

[7] Balanis, C.A., AntennaTheory. 2005, New York: John Wiley & Sons.

[8] Pozar, D., Microstrip Antennas. IEEE Antennas and Propagation Proceeding, 1992.

[9] Krowne, C.M., Cylindrical-Rectangular Microstrip Antenna. IEEE Trans. on Antenna and Propagation, AP-31: pp. 194-199, 1983.

[10] Q. Wu, M. Liu, and Z. Feng, A Millimeter Wave Conformal Phased Microstrip Antenna Array on a Cylindrical Surface. IEEE International Symposium on Antennas and Propagation Society, pp. 1-4, 2008.

[11] J. Ashkenazy, S. Shtrikman, and D. Treves, Electric Surface Current Model for the Analysis of Microstrip Antennas on Cylindrical Bodies. IEEE Trans. on Antenna and Propagation, AP-33: pp. 295-299, 1985.

[12] K. Luk, K. Lee, and J. Dahele, Analysis of the Cylindrical-Rectangular Patch Antenna. IEEE Trans. on Antenna and Propagation. 37: pp. 143-147, 1989.

[13] S. Lei, et al., Anti-impact and Over-loading Projectile Conformal Antennas for GPS,. EEE 3rd International Workshop on Signal Design and Its Applications in Communications, pp. 266-269, 2007.

[14] Kolev, N.Z., Design of a Microstip Conform GPS Patch Antenna. IEEE 17th International Conference on Applied Electromagnetic and Communications, pp. 201-204, 2003

[15] A. Elrashidi, K. Elleithy, and Hassan Bajwa, "The Fringing Field and Resonance Frequency of Cylindrical Microstrip Printed Antenna as a Function of Curvature," International Journal of Wireless Communications and Networking (IJWCN), Jul.-Dec., 2011.

[16] A. Elrashidi, K. Elleithy, and Hassan Bajwa, "Effect of Temperature on the Performance of a Cylindrical Microstrip Printed Antenna for TM01 Mode Using Different Substrates," International Journal of Computer Networks & Communications (IJCNC), Jul.-Dec., 2011.

[17] A. Elrashidi, K. Elleithy, and Hassan Bajwa, "The Performance of a Cylindrical Microstrip Printed Antenna for TM10 Mode as a Function of Temperature for Different Substrates," International Journal of Next-Generation Networks (IJNGN), Jul.-Dec., 2011.

[18] S. M. Wentworth, Applied Electromagnetics, John Wiley & Sons, Sons, New York, 2005.

[19] R. F. Richards, Time-Harmonic Electromagnetic Fields, New York: McGraw-Hill, 1961.

[20] R. Garg, P. Bhartia, I. Bahl, and A. Ittipiboon, Microstrip Antenna Design Handbook, Aetech House, Boston, 2001